Solubility of CO2 in Aqueous Solutions of CaCl2 or MgCl2 and in a Synthetic Formation Brine at Temperatures up to 423 K and Pressures up to 40 MPa

ARTICLE *in* JOURNAL OF CHEMICAL & ENGINEERING DATA · MAY 2013

Impact Factor: 2.04 · DOI: 10.1021/je400396s

3 AUTHORS, INCLUDING:

Danlu Tong
BP plc
6 PUBLICATIONS **50** CITATIONS
SEE PROFILE

David Vega-Maza
University of Aberdeen
13 PUBLICATIONS **115** CITATIONS
SEE PROFILE

Journal of chemical & engineering data

Article

pubs.acs.org/jced

Solubility of CO_2 in Aqueous Solutions of $CaCl_2$ or $MgCl_2$ and in a Synthetic Formation Brine at Temperatures up to 423 K and Pressures up to 40 MPa

Danlu Tong, J. P. Martin Trusler,* and David Vega-Maza

Qatar Carbonates and Carbon Storage Research Centre, Department of Chemical Engineering, Imperial College London, South Kensington Campus, London SW7 2AZ, United Kingdom

ABSTRACT: We report the solubility of carbon dioxide in $CaCl_2$(aq) and $MgCl_2$(aq) at molalities of (1, 3, and 5) mol·kg^{-1}, temperatures of (308 to 424) K and pressures up to 40 MPa. We also report the solubility of CO_2 in a synthetic formation brine containing 0.910 mol·kg^{-1} NaCl and 0.143 mol·kg^{-1} KCl over the same ranges of temperature and pressure. The expanded uncertainties at 95 % confidence are 0.03 K in temperature, between (0.08 and 0.15) MPa in bubble pressure and 0.00015 in the mole fraction of CO_2 in the solution at its bubble point. The results show a strong salting-out effect, whereby the solubility declines with increasing molality of salt, which is some (20 to 30) % greater in $CaCl_2$(aq) or $MgCl_2$(aq) than in the synthetic formation brine at the same molality.

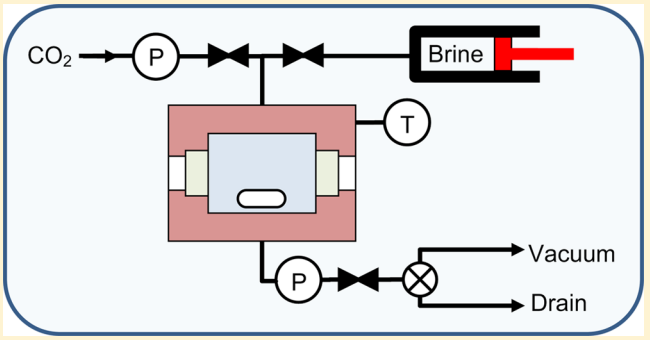

1. INTRODUCTION

The solubility of carbon dioxide in strong electrolytes, especially salty aqueous solutions, plays a key role in numerous processes including CO_2-enhanced oil recovery, the formation of gas hydrates, seawater desalination, and geological carbon storage. In chemical and environmental engineering, geochemical problems and oilfield process engineering, models for the solubility of CO_2 in brines are required in wide ranges of temperature and pressure.[1−7] With respect to carbon capture and storage, deep saline aquifers are thought to be the most promising sinks for CO_2, and modeling the long-term fate of CO_2 in such formations depends greatly upon knowledge of the dissolution equilibria. This arises because solubility trapping of CO_2 in saline aquifers accounts for 90 % of the estimated total storage capacity,[8] solubility being the principal trapping mechanism in the medium term (10^0 to 10^2 years). The solubility of CO_2 in brines depends upon the temperature, pressure, and composition of the brine. Temperatures in reservoirs and deep saline aquifers are typically above 310 K but not usually more than 423 K. With the geothermal temperature gradient of about 30 K·km^{-1} and hydrostatic pressure (or more where the pore space is not connected to the surface), reservoir pressures above 8 MPa are typical.[9] Hence, under these conditions, CO_2 is in a supercritical state. The salinity of reservoir brines usually increases with depth up to about 400 g·L^{-1}.[10]

Examination of the literature shows that the solubility of CO_2 in NaCl (aq) and KCl (aq) has been well studied at pressures up to about 10 MPa.[1,11−13] There also exist some elevated-pressure solubility data for CO_2 in aqueous solutions of K_2CO_3,[13] $CaCl_2$,[12,14−16] and Na_2SO_4.[17,18] A large body of data exists for CO_2 solubility in other aqueous strong electrolyte solutions but this is generally restricted to ambient or near-ambient pressures and, often, to rather restricted ranges of temperature. Given the relative lack of data for CO_2 solubility in important alkaline-earth halides at reservoir conditions, especially with respect to $MgCl_2$ and $CaCl_2$, the available models for CO_2 solubility in formation brines are not well validated for brines rich in these species. Thus there is a need for new measurement which we start to address in this work.

In this paper, we describe a new synthetic apparatus for studying solubility in electrolyte systems of the type (CO_2 + brine) at reservoir conditions. Solubility data are reported over wide ranges of temperature and pressure for CO_2 in both a simplified synthetic formation brine, {NaCl (b = 0.910 mol·kg^{-1}) + KCl (b = 0.143 mol·kg^{-1})}(aq), and in $CaCl_2$(aq) and $MgCl_2$(aq) at b = (1, 3, and 5) mol·kg^{-1}, where b denotes molality of the salt in water.

2. EXPERIMENTAL SECTION

2.1. Apparatus. Various techniques have been used to determine the solubility of gases in liquids at high pressures, employing either analytical or synthetic methods. The former relies on analyzing a sample of the saturated solution after an equilibrium state is reached.[19−22] In the synthetic method, the compositions are obtained from knowledge of the amount of

Received: April 24, 2013
Accepted: May 20, 2013
Published: May 30, 2013

each component injected into the cell. The measured bubble pressure relates to a state in which a known amount of the gas, previously introduced into the apparatus, is fully dissolved in a measured amount of solvent at the saturation limit.[23] This pressure is found either by visual observation of phase transitions or by volumetric measurements in a blind experiment.[11,17,24]

Concentrated brines are difficult to study experimentally at high temperatures and pressures, primarily because of their corrosive nature. Apart from careful selection of materials, the key is simplicity of approach. Accordingly, the synthetic method based on visual observation and quantitative measurements of temperature, pressure, and composition was employed, avoiding the complications of phase sampling and analysis, and permitting reliable data to be obtained quite rapidly. The view cell where the CO_2 was dissolved in brine was initially filled with a known amount of the gas. During the course of the experiment, the solvent (brine) was injected quantitatively under stirring and with visual observation of the resulting phase behavior up to and beyond the bubble point. Dead volumes were minimized to permit precise determination of the masses present in the cell. As implemented, the apparatus allows gas-solubility to be measured at temperatures up to 473 K with pressures up to 50 MPa. Wetted metallic parts were made from either Hastelloy C276 or titanium, both of which are fairly resistant to corrosion in concentrated brines.

The core of the apparatus, shown schematically in Figure 1, was a windowed autoclave cell (Sitec-Sieber model 740.2225)

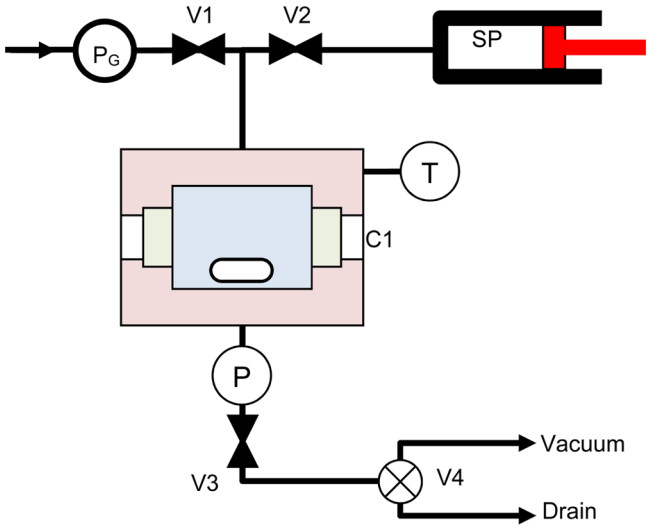

Figure 1. Schematic diagram of the apparatus: C1, windowed autoclave cell with stirrer; SP, high-pressure syringe pump (brine); T, temperature sensor (Pt100); P_G, gas pressure sensor; P, flow-through pressure sensor; V1, high-pressure inlet valve (type 4); V2, high-pressure inlet valve (type 2); V3, high-pressure outlet valve (type 2); V4, 3-port selector valve; V5, rupture-disc safety head (fitted to the main vessel but not shown).

made from Hastelloy C276. This cell was a horizontally orientated cylindrical vessel of 28 mm internal diameter, 40 mm internal length, and nominal volume 25 cm^3. The ends were closed by Hastelloy and sapphire window assemblies, with an optical diameter of 18 mm, which were sealed to the main body by PTFE o-rings as detailed in Figure 2. The cell was equipped with four high-pressure ports for 6.35 mm o.d. conned-and-threaded tubing. Two ports were used for fluid inlet and outlet,

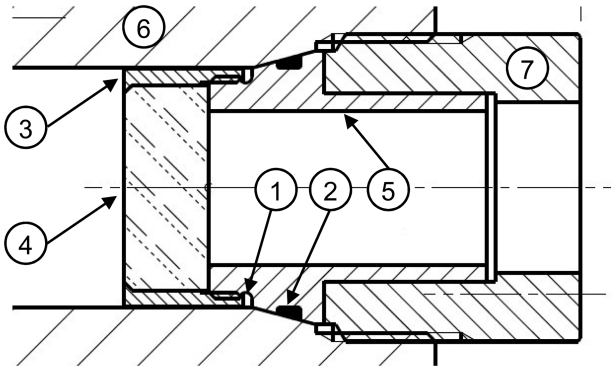

Figure 2. Cross-sectional view of the sapphire window assembly: 1, internal trapped volume; 2, seal recess, filled by PTFE O-ring; 3, retaining ring; 4, sapphire disc; 5; window support (sealed to component 4 by mean of a proprietary bond); 6, cell body; 7, threaded gland.

a third was closed by a rupture-disc safety device, and the fourth was plugged. A blind axial hole in the vessel wall (5 mm diameter × 50 mm long) accommodated a Pt100 temperature sensor. A support system was used to mount the view cell in the center of an air oven with its axis normal to the double-glazed oven door, and an illumination device with diffuser was placed behind the vessel to aid visual observation. Mixing of the cell contents was accomplished by means of an internal PTFE-coated magnetic stirrer bar of ellipsoidal shape (10 mm long × 6 mm diameter), driven by a SmCo magnet assembly mounted on a shaft that passed through a small hole the floor of the oven to a variable-speed electric motor beneath. The stirrer was normally operated at a rotational speed of about 40 s^{-1}.

CO_2 and brine were injected into the cell through the same inlet port, which was fitted with a reducing union and connected to an external three-port type-4 valve by means of Hastelloy C276 tubing of o.d. 1.6 mm and i.d. 0.5 mm which minimized dead volumes in the injection lines. The CO_2 was injected from a gas bottle via a line fitted with a pressure transducer (Omega model PX01K1−750A5T) having a full-scale range of 5.17 MPa. Brine was injected from a syringe pump (Teledyne Isco, model 100DM) made of Hastelloy C276 with a capacity of 100 cm^3, a resolution of 0.01 cm^3, and a maximum working pressure of 69 MPa. The pump was thermostatted by a heating−cooling jacket through which water from a circulating bath was passed at T = 291.15 K. The temperature and pressure of the fluid in the pump were monitored for purposes of determining the density of the brine from an equation of state so that the mass of fluid injected could be computed from the volumetric displacement. A flexible surface-mounted Pt100 temperature sensor affixed to the wall of the cylinder was used to measure the temperature, while a pressure transducer in the head of the pump was used to obtain the pressure.

The outlet port of the cell was also fitted with a reducing union and was connected to an outlet valve by titanium tubing of o.d. 1.6 mm and i.d. 0.5 mm *via* a flow-through pressure transducer (DJ Instruments, model DF2) with titanium wetted parts and a full-scale range of 50 MPa. The location of the pressure transducer was such that it gave a reading of the pressure in the cell substantially unaffected by the pressure drop that develops across the filling line during brine injection.

The temperature on the view cell was controlled by the air oven (Memmert, model UFP 400). The cell temperature

indicated by the Pt100 sensor located in the thermowell was typically constant to within ± 30 mK during a period of 24 h.

The high-pressure syringe pump controlled the pressure of the fluid in the cell when operated in pressure-control mode. A characteristic of the experiment design is that instead of "compressing" the gas into the liquid phase with a movable piston, the liquid phase serves as the moving boundary. Thus it is not only the ever-increasing system pressure which drives dissolution of the gas charge, but also the increasing amount of available solvent.

Leaks are a major concern in this type of system, since the method relies on precise determination of the quantities of materials in the cell. The system was thoroughly leak tested in the whole pressure range with both helium and water and exhibited a high-level of integrity.

2.2. Calibration. The Pt100 thermometer used to measure the cell temperature was calibrated at temperatures in the range (273 to 423) K by comparison in a constant-temperature bath with a standard platinum resistance thermometer having an expanded uncertainty of 2 mK in the present temperature range. Taking sensor drift, and fluctuations and nonuniformity of the air oven into account, we estimate that the overall expanded uncertainty of the cell temperature measurements was 30 mK, with a coverage factor $k = 2$.

The Pt100 sensor used to measure the temperature of the fluid in the syringe pump was not calibrated. On the basis of the manufacturing tolerance, the expanded uncertainty of the pump temperature was taken to be 0.5 K ($k = 2$). The pressure transducer located in the syringe pump was not calibrated by us and the expanded relative uncertainty, based on data provided by the manufacturer, was taken to be 0.5 % ($k = 2$).

The Omega pressure transducer used in the gas filling line was calibrated by the manufacturer prior to the start of this work against instrumentation traceable to the U.S. National Institute of Standards and Technology. The calibration was carried out under vacuum and at 50 % and 100 % of the full-scale pressure. Combined nonlinearity, hysteresis and repeatability errors during calibration were found to be less than 1 kPa, while the specifications of the instrument stated that these errors combined should amount to less than 2.5 kPa. The overall expanded uncertainty of the gas-pressure measurements was estimated to be 2 kPa ($k = 2$).

The model DF2 flow-through pressure transducer was calibrated against a hydraulic pressure balance (DH-Budenberg model 580EHX) having an expanded relative uncertainty of 0.008 %. In the calibration, the transducer exhibited good linearity and a lack of hysteresis, leading to an expanded uncertainty of 11 kPa. However, this sensor did drift over time and corrections were required. For this purpose, the DF2 transducer was compared in each experiment with the more-stable Omega pressure transducer after charging the system with CO_2. Any difference was applied as a constant offset to correct subsequent readings in that run. Taking all factors into account, the expanded uncertainty of the pressure in the cell during and after brine injection was estimated to be 70 kPa ($k = 2$).

The volumes of the cell, inlet and outlet lines and safety head were needed for determining the initial amount of gas. This was determined by injecting pure water at a reference pressure p_{ref} = 1 MPa and reference temperature T_{ref} = 323.15 K. The density of water at this temperature is known with a relative uncertainty of 0.001 %.[25] The volume of the system obtained, V_{ref} = (27.182 ± 0.012) cm^3 ($k = 2$), includes the volumes in the inlet and outlet lines. These small volumes, amounting in total to about 1 % of the system volume, were dimensionally characterized with an uncertainty of 0.014 cm^3 ($k = 2$). The volume was corrected for the effect of thermal expansion according to the relation

$$V(T, p) = V_{ref}[1 + \alpha_V(T - T_{ref})] \quad (1)$$

where α_V is the mean volumetric expansivity. This was taken to be 36 × 10^{-6} K^{-1}, three times the linear thermal expansion coefficient of Hastelloy C276.[26] Thus, a change in temperature of 100 K yields a calculated relative change in volume of 0.36 %. The dilation of the cell under the greatest pressure was estimated to amount to less than 0.03 % of the volume and was neglected.

2.3. Internal Dead Volume. During validation experiments, it became apparent that, in addition to the volumes in the inlet and outlet lines, there was a small additional dead volume within the cell that was filled with water during the calibration, before which the cell was evacuated, but not filled with water or brine during a CO_2 solubility experiment. This dead volume, amounting to a total of 0.20 cm^3, was associated with the sapphire window assemblies, details of which are shown in Figure 2. It can be seen that the sapphire discs were retained against the Hastelloy body of the window assembly by means of a threaded ring. Behind the threaded ring there was an annular void, the volume of which was determined by careful measurements to be 0.10 cm^3 for each window assembly. During a solubility measurement, gas could enter this space via the annular clearance between the o.d. of the threaded ring and the i.d. of the cell. However, water or brine could not enter this space because, despite the high total pressure, the differential pressure between the void and the bulk of the cell volume, being just the hydrostatic head over the cell diameter, was always less than the capillary entry pressure Δp_c estimated from the Young−Laplace equation for parallel plates:

$$\Delta p_c = (2\gamma/d)\cos\theta \quad (2)$$

Here, γ is the interfacial tension, d is the width of the annular space around the o.d. of the window and θ is the contact angle. For CO_2−brine systems in the ranges of temperature and pressure investigated here, $\gamma \geq 30$ mN·m^{-1} and the contact angle on metallic surfaces ≤45°,[27−29] while, from mechanical measurements on the windows and cell, $d \leq 0.1$ mm. Hence $\Delta p_c \geq 400$ Pa which is greater than the maximum possible hydrostatic head during brine injection. Other possible trapped volumes were considered but found to be negligible.

2.4. Materials. Pure deionized and degassed water (electrical resistivity >18 MΩ·cm at T = 298.15 K) was used. Carbon dioxide was supplied by BOC with a specific minimum mole fraction purity of 0.99995, and was used as supplied. A 0.5 μm pore size particulate filter was fitted in the gas line. Sodium chloride and potassium chloride were purchased from Sigma-Aldrich, with mass fraction purities of ≥ 0.995 and ≥ 0.99, respectively. Both salts were dried in an oven at T = 373.15 K and at ambient pressure. Calcium chloride hexahydrate, $CaCl_2{\cdot}6(H_20)$, and magnesium chloride hexahydrate, $MgCl_2{\cdot}6(H_20)$, were purchased from VWR. The manufacturer certified that the mass fraction of $CaCl_2$ or $MgCl_2$ was between 99 % and 102 % of that of the pure hexahydrate, as determined by titration with EDTA. No analysis or purification was attempted. However, since these salts, especially the hexahydrates, present

hygroscopic behavior, care was taken to avoid more than momentary contact with air.

Solutions were prepared gravimetrically with the relative uncertainties in mass being below 0.01 %. Thus the uncertainty of molality was most probably limited by the purity of the salts and was taken to be approximately 0.5 % for the NaCl and (NaCl + KCl) solutions and 2 % for the $CaCl_2$ and $MgCl_2$ solutions.

2.5. Experimental Procedure. The previously evacuated cell was first filled with CO_2. Once equilibrium was reached, the temperature and pressure were measured so that the mass of CO_2 present could be determined by means of an equation of state[30] and knowledge of the volume. Brine was then injected, stepwise, from the high-pressure syringe pump until the gas was entirely dissolved under stirring. Quantitative determination of the mass of brine injected was accomplished knowing the initial and final values of volume, temperature, and pressure in the pump cylinder together with the density of the brine under those conditions.

For systems in which the solubility is a strong function of pressure, for example, those that follow Henry's law, the bubble point could be determined easily in a blind experiment from the abrupt change in the slope of pressure versus mass of injected brine. However, the solubility of CO_2 in water or brines tends to a limiting value at high pressures and the bubble-point can then no longer be determined precisely in a blind experiment. However, visual observation allows the bubble point to be located even at high pressures. The time constant for the approach to thermodynamic equilibrium either in the one-phase or the two-phases regions was found to be around 3 h. Hence, the time required for full stabilization after an injection of brine could be long. To accomplish an experiment within 24 h, brine was first injected slowly until a pressure slightly in excess of the anticipated bubble point was reached, and the system was mixed for about 12 h. After this, the pressure was slowly decreased by withdrawing some fresh brine from the inlet line (not in contact with the CO_2), using the pump, until the first stable bubbles appeared. Backlash on the pump was taken into account. At high pressures, the phase boundary was observed first as slight spatial and temporal variations in the light passing though, rather than by actual bubble formation. This is because, in these thermodynamic states, the density of the incipient CO_2-rich phase is comparable to that of the brine. The composition of the solution at the bubble point was computed from the known masses of CO_2 and brine present as detailed below. Since the cell volume was also known, it was possible to estimate the density of the CO_2-saturated brine at the bubble point.

2.6. Analysis. To analyze the experimental data for solubility, we consider the apparatus as comprising five regions identified by subscripts 0, 1, 2, 3, and 4 that refer to the optical cell, the internal dead volume, the pump cylinder, the inlet line, and the outlet line respectively. In the following, we use subscripts "g" for gas/solute (CO_2), "s" for solvent (brine), "w" for pure water, and "salt" for pure salt; additionally, subscripts "i" and "f" refer to the initial and final pressures in an experiment. For a measurement run, the p_i is the gas filling pressure and the p_f is the bubble pressure.

Since all of the gas initially in the inlet line (volume V_3) is pushed into the cell by the brine, the mass of solute finally in the cell and available to dissolve in the solvent is the mass initially in the cell plus the mass initially in V_3 less the mass finally in dead volume V_1:

$$m_g = \rho_g(T_0, p_i)V_0 + \rho_g(T_3, p_i)V_3 - \rho_g(T_0, p_f)V_1 \quad (3)$$

where ρ is density and V_0 is the volume of the cell. The mass of solvent finally in the cell is the mass displaced by the pump less the mass in the inlet and outlet lines (assuming that the outlet line, volume V_4, fills with fresh brine as soon as brine injection starts):

$$m_s = [\rho_s(T_2, p_f)V_{2,f} - \rho_s(T_2, p_i)V_{2,i}] - [\rho_s(T_3, p_f)V_3 + \rho_s(T_4, p_f)V_4] \quad (4)$$

The cell volume V_0 comes from the calibration experiment with pure water and the calculated thermal expansion according to eq 1 with

$$V_{ref} = \{[\rho_w(T_2, p_f)V_{2,f} - \rho_w(T_2, p_i)V_{2,i}] - [\rho_w(T_3, p_f)V_3 + \rho_w(T_4, p_f)V_4]\}/\rho_w(T_{ref}, p_f) \quad (5)$$

In eq 5, the initial and final states refer to the initial and final pump pressures in the calibration run, and T_{ref} is the temperature of the cell during calibration. Finally, the composition at the bubble point, expressed in terms of the salt-free mole fraction of dissolved gas x', is given by

$$x' = \frac{n_g}{n_g + n_w} = \frac{m_g}{m_g + m_s(M_g/M_w)(1 + bM_{salt})^{-1}} \quad (6)$$

Here, n denotes amount of substance and M denotes molar mass. For a solution containing N different salts each of molality b_i and molar mass M_i, we have:

$$bM_{salt} = \sum_{i=1}^{N} b_i M_i \quad (7)$$

To estimate the uncertainty of x', the contribution associated with each input quantity appearing in eqs 3 to 7 was determined numerically. The parameters considered were the temperatures, the extraneous volumes V_1, V_2, V_3, and V_4, and the densities of CO_2, brine, and water. There was also a subjective uncertainty associated with visual identification of the bubble-point condition, and this term dominates the uncertainty of the measured bubble pressure.

A key feature of the method is that any constant relative systematic error in the pump displacement cancels out in first order because the pump was used both for volume calibration and for the measurement. However, in estimating the overall uncertainties, we allowed for 0.3 % relative uncertainty in the dispensed volumes during both calibration and measurement.

The analysis yields a combined expanded uncertainty in the salt-free mole fraction x' of 0.00015. The uncertainties of the bubble pressures p_b were 0.15 MPa for $p_b \leq 8$ MPa; 0.2 MPa for the interval (8 MPa $\leq p_b \leq$ 25 MPa); and 0.3 MPa for $p_b >$ 25 MPa. All reported uncertainties are expanded values with a coverage factor $k = 2$, and were calculated following the recommendations of EA-4/02.[31] We note that, in principle, the experimental method permits determination of the density of the solution at the bubble point from m_g, m_s, and V_0. However, we estimated the relative uncertainty to be approximately 0.6 % and therefore choose not to report densities.

2.7. Validation. The solubility of CO_2 in water was measured at $T = 373$ K for five initial gas filling pressures. The density of water was obtained from the IAPWS-1995 equation of state[25] and used to meter the amount of solvent injected at

pump conditions. The results are presented in Table 1 and Figure 3 together with data from the literature.[11,15,32,33] Figure 3 includes also the solubility calculated from the model of Duan et al.[34] which is an improvement over a previous version[35] with noniterative equations to calculate the CO_2 fugacity coefficients. The present results are in good agreement with the most of the literature and are especially close to the experimental data of Hou et al.,[33] which were obtained by the analytical method, and the predictions of the model of Duan et al.[34] The results of Wiebe et al.[33] and Prutton et al.[15] generally agree to within ± (2 to 5) % in mole fraction at a given pressure. It is worth noting that both analyzed a saturated sample by evolving the CO_2 at atmospheric pressure in a gas buret and weighing the remaining solution. The results of Kiepe et al.[11] tend to overestimate the solubility at given pressure by as much as 15 %. The latter used a static technique based on volumetric measurements in a blind experiment.

Table 1. Solubility of CO_2 in Water at Temperatures T and Pressures p, Expressed As Mole Fraction x of CO_2 Water at the Bubble Point.[a] Comparison with Interpolated Values from the Literature: Kiepe *et al.*;[11] Wiebe *et al.*;[32] Prutton *et al.*;[15] Hou *et al.*[33]

water (this work)			ref 11	ref 32	ref 15	ref 33
T/K	p/MPa	x	x	x	x	x
374.41	7.21	0.0110	0.013	0.0113	0.0120	0.0110
374.18	14.44	0.0171		0.0175	0.0181	0.0170
374.91	18.86	0.0192		0.0198	0.0201	
374.15	22.34	0.0205		0.0211	0.0212	
374.99	27.26	0.0219		0.0226	0.0223	

[a]Combined expanded uncertainties are $U(T)$ = 0.03 K, $U(x')$ = 0.0001, and $U(p)$ = 0.15 MPa for $p \leq 8$ MPa, or $U(p)$ = 0.20 MPa for (8 MPa < $p \leq$ 25 MPa), or $U(p)$ = 0.30 MPa for p > 25 MPa.

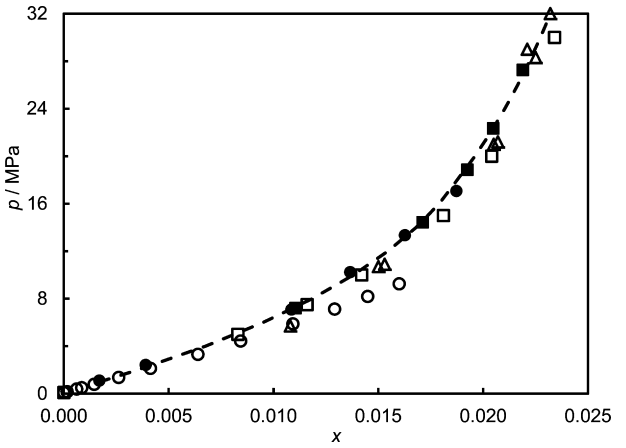

Figure 3. Comparison of the literature data for the solubility of CO_2 in water at T = 373.15 K with the experimental values obtained in this work, x is mole fraction of CO_2 in water: ■, this work; ○, Kiepe et al.;[11] □, Wiebe et al.;[32] △, Prutton et al.;[15] ●, Hou et al.;[33] ---, model of Duan et al.[34]

3. RESULTS AND DISCUSSION

3.1. Synthetic Formation Brine. The solution {NaCl (w = 0.05) + KCl (w = 0.01)}(aq), where w denotes mass fraction, was chosen for the initial study as this brine is similar to some formation brines and has been used in laboratory core-flooding and micro-CT studies of flow in porous media.[36] The precise composition of the brine in molality units was b(NaCl) = 0.910 mol·kg^{-1} and b(KCl) = 0.143 mol·kg^{-1} giving a total molality b = 1.053 mol·kg^{-1}. The density of the brine under the conditions in the syringe pump was taken from measurements recently carried out in our laboratory on the same brine using a vibrating-tube densimeter.[37] The overall expanded relative uncertainty of the brine density under the conditions in the pump was 0.1 %. The CO_2-solubility was measured at five nominal temperatures, T = (309, 324, 344, 375 and 425) K, with different CO_2 filling pressures resulting in 14 solubility points for this brine which are reported in Table 2 expressed as pressure p and mole fraction x' of dissolved CO_2 on a salt-free basis at each measured bubble point. Figure 4 shows our experimental bubble-point pressures as functions of salt-free mole fraction and include the vapor pressure of pure water at different temperatures as an approximation to the saturation pressure at $x' \rightarrow 0$.[25] We see that the bubble-pressure curves tend toward limiting values of solubility at high pressures. We also show in Figure 4 the solubility calculated from the model of Duan et al.,[34] and the agreement is generally good.

Table 2. Solubility of CO_2 in {NaCl(b = 0.910 mol·kg^{-1}) + KCl(b = 0.143 mol·kg^{-1})}(aq), where b Denotes Molality of Salt in Water at Temperatures T and Pressures p, Expressed As Mole Fraction x' of CO_2 in Salt-Free Water at the Bubble Point[a]

T/K	p/MPa	x'	T/K	p/MPa	x'
309.14	1.192	0.0038	374.92	2.99	0.0041
308.90	3.737	0.0118	374.92	6.96	0.0087
			374.89	14.78	0.0142
324.11	1.07	0.0032			
324.10	4.35	0.0106	424.67	4.00	0.0041
			424.62	8.68	0.0087
343.83	1.77	0.0030	424.64	17.16	0.0146
343.92	3.61	0.0064			
345.04	10.25	0.0138			
343.88	13.69	0.0158			

[a]Combined expanded uncertainties are $U(b)$ = 0.005b, $U(T)$ = 0.03 K, $U(x')$ = 0.0001 and $U(p)$ = 0.15 MPa for $p \leq$ 8 MPa or $U(p)$ = 0.20 MPa for p > 8 MPa.

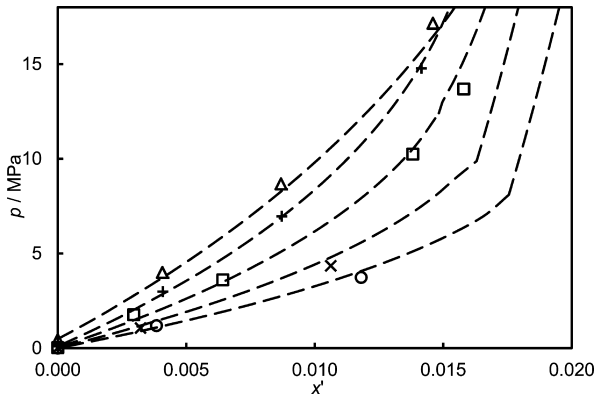

Figure 4. Solubility of CO_2 in {NaCl(b = 0.910 mol·kg^{-1}) + KCl(b = 0.143 mol·kg^{-1})}(aq) where b is molality of salt in water and x' is mole fraction of CO_2 in salt-free water: ○, T = 309 K; ×, T = 324 K; □, T = 344 K; +, T = 375 K; △, T = 425 K; ---, model of Duan et al.[34]

Table 3. Solubility of CO_2 in $CaCl_2$(aq) of Molality b = (1, 3, 5) mol·kg^{-1} at Temperatures T and Pressures p, Expressed As Mole Fraction x' of CO_2 in Salt-Free Water at the Bubble Point.[a]

b = 1 mol·kg^{-1}			b = 3 mol·kg^{-1}			b = 5 mol·kg^{-1}		
T/K	p/MPa	x'	T/K	p/MPa	x'	T/K	p/MPa	x'
309.67	1.53	0.0045	309.61	2.73	0.0036	309.70	4.54	0.0031
309.28	4.01	0.0104	309.63	6.59	0.0078	309.74	23.00	0.0046
309.28	7.67	0.0161	309.59	26.00	0.0081	308.00	24.25	0.0049
344.67	2.58	0.0040	344.80	3.93	0.0032	344.72	6.12	0.0027
344.35	7.30	0.0098	344.95	13.91	0.0068	344.70	14.54	0.0036
344.95	31.02	0.0151	345.08	34.43	0.0078	344.96	34.52	0.0051
374.70	3.13	0.0038	374.65	5.99	0.0036	374.72	7.61	0.0027
374.70	10.02	0.0093	374.80	15.72	0.0064	374.72	16.91	0.0040
374.88	37.38	0.0161	374.80	33.45	0.0077	374.72	34.25	0.0048
424.13	4.39	0.0039	424.40	8.29	0.0038	424.43	4.64	0.0014
424.10	12.77	0.0100	424.39	27.11	0.0081	424.42	10.53	0.0024
424.43	26.82	0.0158	424.38	37.99	0.0090	424.64	29.41	0.0048

[a]Combined expanded uncertainties are $U(b) = 0.02b$, $U(T) = 0.03$ K, $U(x') = 0.0001$, and $U(p) = 0.15$ MPa for $p \leq 8$ MPa, or $U(p) = 0.20$ MPa for (8 MPa < $p \leq 25$ MPa), or $U(p) = 0.30$ MPa for $p > 25$ MPa.

Table 4. Solubility of CO_2 in $MgCl_2$(aq) of Molality b = (1, 3, 5) mol·kg^{-1} at Temperatures T and Pressures p, Expressed As Mole Fraction x' of CO_2 in Salt-Free Water at the Bubble Point.[a]

b = 1 mol·kg^{-1}			b = 3 mol·kg^{-1}			b = 5 mol·kg^{-1}		
T/K	p/MPa	x'	T/K	p/MPa	x'	T/K	p/MPa	x'
309.58	1.25	0.0038	310.00	2.84	0.0036	309.68	3.50	0.0027
309.83	4.24	0.0108	309.91	6.00	0.0065	309.74	9.00	0.0049
309.81	7.74	0.0175	309.91	11.20	0.0079	309.52	31.02	0.0056
			309.91	20.72	0.0092			
343.90	2.04	0.0034				344.68	5.80	0.0028
344.20	7.62	0.0100	345.06	4.05	0.0032	344.68	6.00	0.0028
344.93	30.58	0.0153	344.98	13.12	0.0068	344.68	13.09	0.0037
			345.01	31.25	0.0080	344.98	31.20	0.0047
374.24	2.64	0.0029						
374.22	10.25	0.0100	374.84	4.95	0.0033	374.72	7.55	0.0026
374.91	34.93	0.0161	374.90	15.16	0.0064	374.68	15.60	0.0038
			374.83	26.29	0.0080	375.02	20.58	0.0041
424.03	3.95	0.0035						
423.95	12.63	0.0098	424.60	7.60	0.0033	424.39	4.70	0.0013
424.63	19.74	0.0131	424.65	19.20	0.0063	424.33	10.34	0.0023
424.63	28.37	0.0161	424.68	31.71	0.0079	424.49	16.18	0.0035

[a]Combined expanded uncertainties are $U(b) = 0.02b$, $U(T) = 0.03$ K, $U(x') = 0.0001$, and $U(p) = 0.15$ MPa for $p \leq 8$ MPa, or $U(p) = 0.20$ MPa for (8 MPa < $p \leq 25$ MPa), or $U(p) = 0.30$ MPa for $p > 25$ MPa.

3.2. $CaCl_2$(aq) and $MgCl_2$(aq). $CaCl_2$(aq) and $MgCl_2$(aq) were studied at molalities of (1, 3 and 5) mol·kg^{-1} and at nominal temperatures of T = (309, 345, 375 and 424) K, with three or four different initial CO_2 filling pressures at each temperature and molality. As before, the density of the brines under the conditions in the syringe pump were taken from measurements recently carried out in our laboratory on the same solutions using a vibrating tube densimeter and are burdened by relative uncertainties of 0.1 % (k = 2).[37] The experimental results are reported in Tables 3 and 4 and plotted in Figure 5. The vapor pressures of each brine calculated from ref 38 are also plotted to represent the bubble pressure at infinite dilution of CO_2. The qualitative trends are generally as expected: the solubility decreases with increasing temperature and increases with increasing pressure, tending toward a limiting value at very high pressures. However, the temperature dependence reverses at high pressures and temperatures, to increasing solubility with increasing temperature, as observed by other authors.[15,32,34] The salting-out effect is also seen to be very strong in these systems and to be almost the same in $MgCl_2$(aq) as it is in $CaCl_2$(aq). It is worth noting that the two parameters influencing the thermodynamic behavior of strong electrolytes are ion concentration and ion charge.[39] Alkali metal halides are rather well studied, whereas data for the alkali-earth halides are sparse and such data are required to understand specific behavior according with the type of salt. In comparison with the NaCl/KCl mixed brine discussed above, the 1 mol·kg^{-1} $CaCl_2$ and $MgCl_2$ solutions have bubble pressures that are (20 to 30) % higher for the same concentration of dissolved CO_2. Thus the salting-out effect is significantly greater in these systems with divalent cations.

Numerous thermodynamic models have been used to describe the solubility behavior of CO_2 and other supercritical components in aqueous electrolytes. In the present work, we sought a simple correlative model and, for that purpose, the Krichevsky−Kasarnovsky (KK) equation is a favorable choice:

$$\ln(f_1/x_1) = \ln H_{12} + V_1^{\infty}(p - p_{ref})/(RT) \quad (8)$$

dx.doi.org/10.1021/je400396s | J. Chem. Eng. Data 2013, 58, 2116−2124

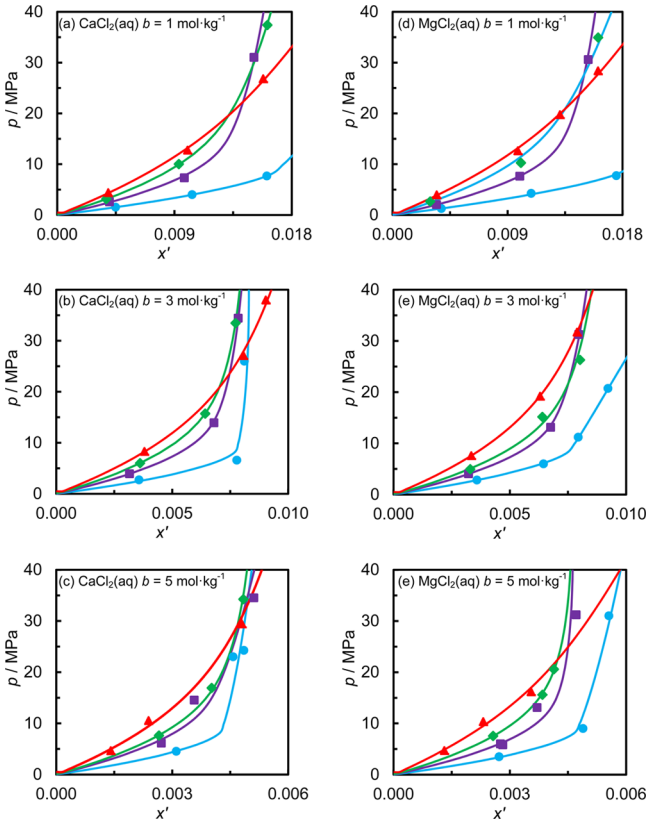

Figure 5. Solubility of CO_2 in $CaCl_2$(aq) and $MgCl_2$(aq) at molalities b = (1, 3, 5) mol·kg^{-1}, where x' is the mole fraction of CO_2 in salt-free water and b is the molality of salt in water. Symbols: blue ●, T = 309 K; purple ■, T = 345 K; green ◆, T = 375 K; red ▲, T = 424 K; Solid lines are fits to the Krichevsky–Kasarnovski model.

Here, f_1 is the partial fugacity of CO_2 (component 1) in the vapor phase, x_1 is the mole fraction of CO_2 in the liquid phase, H_{12} is Henry's constant for CO_2 in the brine phase, V_1^∞ is the partial molar volume of CO_2 at infinite dilution in the aqueous phase, and p_{ref} is the vapor pressure of the brine at the temperature in question. In this analysis, the brine is treated as a single pseudocomponent, the activity coefficient of CO_2 in aqueous solution is taken to be unity and the partial molar volume V_1^∞ is taken to be independent of pressure. We further approximated the partial fugacity of CO_2 in the vapor phase by the fugacity of pure CO_2 at the same temperature and pressure, which was evaluated from the equation of state of Span and Wagner,[30] and set $x_1 = x'$. Thus, to fit the solubility data on a single isotherm, H_{12} and V_1^∞ are the parameters to be regressed. Equation 8 has been fitted to the data measured for each brine on each isotherm and the resulting values of H_{12} and V_1^∞ are given in Table 5. The solubilities according to the KK equation with these values of H_{12} and V_1^∞ are also plotted in Figure 5. The quality of the fits, as measured by the average absolute deviation $\Delta_{x'}$ of x' are generally good. However, we note that the results conform to the KK equation less well at T = 345 K and b = 5 mol·kg^{-1} for both $CaCl_2$(aq) and $MgCl_2$(aq).

The KK approach is expected to be increasingly accurate at low pressures and the fitted values of the Henry's law constant are therefore considered to be reliable within a probably relative uncertainty of about 5 %. The values of ln(H_{12}) obtained are shown in Figure 6 as functions of inverse temperature, for both

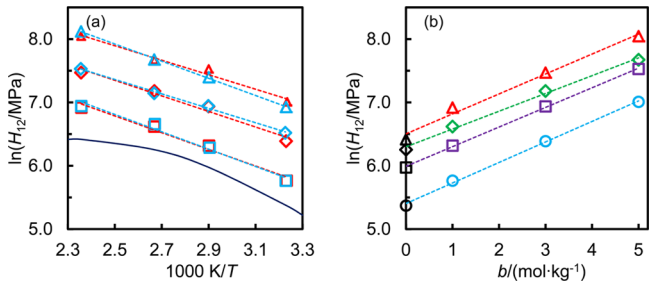

Figure 6. Dependence of Henry's constant H_{12} of CO_2 (1) in water or $CaCl_2$(aq) or $MgCl_2$(aq) (2) upon temperature T and molality b of salt in water. (a): $H_{12}(T)$ for CO_2 in CaCl2(aq) (red □, b = 1 mol·kg^{-1}; red ◇, b = 3 mol·kg^{-1}; red △, b = 5 mol·kg^{-1}), $MgCl_2$(aq) (blue □, b = 1 mol·kg^{-1}; blue ◇, b = 3 mol·kg^{-1}; blue △, b = 5 mol·kg^{-1}) and pure water (—, from Harvey[40]). (b) $H_{12}(b)$ for CO_2 in $CaCl_2$(aq) (blue ○, T = 309 K; purple □, T = 345 K; green ◇, T = 375 K; red △, T = 424 K) and in pure water (black symbols, from Harvey[40]).

Table 5. Fitted Parameters in the Krichevsky–Kasarnovsky Model. H_{12} is Henry's constant of CO_2 in Aqueous Solution; V_1^∞ is the Partial Molar Volume of CO_2 in the Aqueous Solution at Infinite Dilution; and $\Delta_{x'}$ is the Average Absolute Deviation of Mole Fraction x' of CO_2 in Salt-Free Water at the Bubble Point

T/K	H_{12}/MPa	V_1^∞/(cm^3·mol^{-1})	$\Delta_{x'}$	T/K	H_{12}/MPa	V_1^∞/(cm^3·mol^{-1})	$\Delta_{x'}$
	$MgCl_2$(aq), b = 1 mol·kg^{-1}				$CaCl_2$(aq), b = 1 mol·kg^{-1}		
309.74	318			309.41	319		
344.34	537	41.1	0.0001	344.66	554	39.3	0.0002
374.46	780	29.8	0.0004	374.76	749	36.5	0.0001
424.31	1036	20.4	0.0002	424.22	1010	22.3	0.0001
	$MgCl_2$(aq), b = 3 mol·kg^{-1}				$CaCl_2$(aq), b = 3 mol·kg^{-1}		
309.93	679	14.5	0.0001	309.61	595	45.6	0.0004
345.02	1038	41.0	0.0001	344.94	1030	44.3	0.0001
374.86	1269	46.7	0.0002	374.75	1313	49.7	0.0001
424.64	1865	44	0.0001	424.39	1757	41.8	0.0001
	$MgCl_2$(aq), b = 5 mol·kg^{-1}				$CaCl_2$(aq), b = 5 mol·kg^{-1}		
309.65	1021	33.4	0.0001	309.15	1107	37.1	0.0001
344.76	1632	50.3	0.0002	344.79	1861	33.5	0.0003
374.81	2158	53.9	0.0000	374.72	2149	48.0	0.0001
424.40	3363	25.1	0.0001	424.50	3120	40.3	0.0001

dx.doi.org/10.1021/je400396s | J. Chem. Eng. Data 2013, 58, 2116–2124

the $CaCl_2$(aq) and $MgCl_2$(aq) systems, and of molality for the $CaCl_2$(aq) system. In the range of conditions studied, $\ln(H_{12})$ appears to be a linear function of inverse temperature and a linear function of molality for both brine systems. The correlation reported by Harvey[40] for CO_2 in pure water is also plotted in Figure 6 but this shows significant curvature of $\ln(H_{12})$ as a function of inverse temperature. The approximations involved in the KK approach are known to be limiting at high pressures and temperatures[41] and so the infinite-dilution partial molar volumes obtained in the fitting are best thought of as empirical parameters. The values reported in Table 5 may be compared with those for CO_2 in pure water[42] which increase from 34 $cm^3 \cdot mol^{-1}$ at T = 309 K to 43 $cm^3 \cdot mol^{-1}$ at T = 424 K.

The present results are not easily compared directly with the few available data in the literature[12,14−16] as they pertain to different state points. However, the new data may be compared easily with the model of Duan et al.[34] Since the results for $CaCl_2$(aq) and $MgCl_2$(aq) are almost identical, we restrict our comparison, shown in Figure 7, to the former at molalities of (1 and 5) $mol \cdot kg^{-1}$. The model is known to perform well for CO_2 in pure water and it is not surprising that it also describes the more dilute brine system rather well. The one obvious failure of the model at low salt molality is observed at the lowest temperature, where the model turns upward prematurely with increasing x'. The model is also seen to perform quite well for the most concentrated brine studied in this work with the same exception at the lowest temperature. Similar agreement was found at b = 3 $mol \cdot kg^{-1}$.

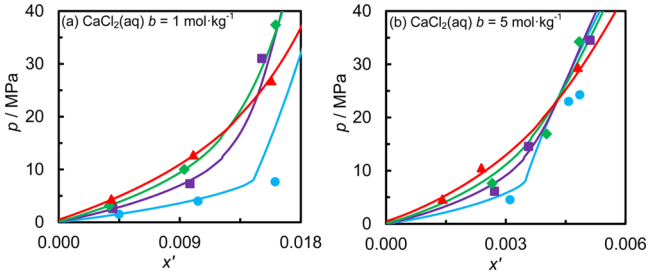

Figure 7. Solubility of CO_2 in $CaCl_2$(aq) at molalities b = (1 and 5) $mol \cdot kg^{-1}$, where x' is the mole fraction of CO_2 in salt-free water and b is the molality of salt in water. This work: blue ●, T = 309 K; purple ■, T = 345 K; green ◆, T = 375 K; red ▲, T = 424 K. Solid lines are computed from the model of Duan et al.[34].

4. CONCLUSIONS

A synthetic method based on quantitatively determination of solute and solvent masses and visual observation of phase transitions has been implemented, along with an appraisal of the uncertainties in solubility measurements by this technique. The apparatus is suitable for studying CO_2 solubility in mixed-electrolyte solutions at temperatures up to 473 K and pressures up to 50 MPa. The technique has been validated by means of a measurement on the well-studied (CO_2 + water) system. CO_2 solubility data are reported at 14 state points in the NaCl/KCl mixed brine, 36 points in $CaCl_2$(aq), and 38 points in $MgCl_2$(aq). The results significantly expand the range of states (temperature, pressure, and molality) over which the solubility of CO_2 in these brines is known. We find a strong salting out effect which is greater in the systems with divalent cations than in the monovalent NaCl/KCl mixed brine. At the same time, the solubility of CO_2 in $CaCl_2$ and $MgCl_2$ brines of the same molality was found to be very similar. We can conclude that ion charge is overwhelmingly more important than ion size in relation to the salting out effect in these aqueous strong electrolyte systems. The results are in generally good agreement with the empirical model of Duan et al.,[34] except at the lowest temperature studied where the model underestimates the solubility of CO_2 in $CaCl_2$(aq) and $MgCl_2$(aq).

AUTHOR INFORMATION

Corresponding Author

*E-mail: m.trusler@imperial.ac.uk.

Funding

This work was carried out as part of the Imperial College—Shell Grand Challenge Program on Clean Fossil Fuels. The authors gratefully acknowledge Shell International Exploration and Production B.V. for supporting the present project and for permission to publish this research.

Notes

The authors declare no competing financial interest.

REFERENCES

(1) Rumpf, B.; Nicolaisen, H.; Ocal, C.; Maurer, G. Solubility of carbon dioxide in aqueous solutions of sodium chloride: Experimental results and correlation. *J. Sol. Chem.* **1994**, *23*, 431−448.

(2) Hu, J.; Duan, Z.; Zhu, C.; Chou, I. PVTx properties of the CO_2−H_2O and CO_2−H_2O−NaCl systems below 647 K: Assessment of experimental data and thermodynamic models. *Chem. Geol.* **2007**, *238*, 249−267.

(3) Nighswander, J. A.; Kalogerakis, N.; Mehrotra, A. K. Solubilities of carbon dioxide in water and 1 wt % sodium chloride solution at pressures up to 10 MPa and temperatures from 80 to 200 °C. *J. Chem. Eng. Data* **1989**, *34*, 355−360.

(4) Wang, L.−S.; Lang, A.−X.; Guo, T.-M. Measurement and correlation of the diffusion coefficients of carbon dioxide in liquid hydrocarbons under elevated pressures. *Fluid Phase Equilib.* **1996**, *117*, 364−372.

(5) Li, Z.; Dong, M.; Li, S.; Dai, L. Densities and solubilities for binary systems of carbon dioxide + water and carbon dioxide + brine at 59 °C and pressures to 29 MPa. *J. Chem. Eng. Data* **2004**, *49*, 1026−1031.

(6) Ota, M.; Abe, Y.; Watanabe, M.; Smith, R. L. J.; Inomata, H. Methane recovery from methane hydrate using pressurized CO_2. *Fluid Phase Equilib.* **2005**, *228*, 553−559.

(7) White, C. M.; Smith, D. H.; Jones, K. L.; Goodman, A. L.; Jikich, S. A.; LaCount, R. B.; DuBose, S. B.; Ozdemir, E.; Morsi, B. I.; Schroeder, K. T. Sequestration of carbon dioxide in coal with enhanced coalbed methane recovery—A review. *Energy Fuels* **2005**, *19*, 659−724.

(8) Shukla, R.; Ranjith, P.; Haque, A.; Choi, X. A review of studies on CO_2 sequestration and caprock integrity. *Fuel* **2010**, *89*, 2651−2664.

(9) Holloway, S. Carbon dioxide capture and geological storage. *Phil. Trans. R. Soc. A* **2007**, *365*, 1095−1107.

(10) Bachu, S.; Bennion, D. B. Interfacial tension between CO_2, freshwater, and brine in the range of pressure from (2 to 27) MPa, temperature from (20 to 125) °C, and water salinity from (0 to 334 000) $mg \cdot L^{-1}$. *J. Chem. Eng. Data* **2009**, *54*, 765−775.

(11) Kiepe, J.; Horstmann, S.; Fischer, K.; Gmehling, J. Experimental determination and prediction of gas solubility data for CO_2 + H_2O mixtures containing NaCl or KCl at temperatures between 313 and 393 K and pressures up to 10 MPa. *Ind. Eng. Chem. Res.* **2002**, *41*, 4393−4398.

(12) Malinin, S. D.; Saveleva, N. I. The solubility of CO_2 in NaCl and $CaCl_2$ solutions at 25, 50 and 75 °C under elevated CO_2 pressures. *Geochem. Int.* **1972**, *9*, 410−418.

(13) Kamps, A. P. S.; Meyer, E.; Rumpf, B.; Maurer, G. Solubility of CO_2 in aqueous solutions of KCl and in aqueous solutions of K_2CO_3. *J. Chem. Eng. Data* **2007**, *52*, 817−832.
(14) Malinin, S. D.; Kurovskaya, N. A. Solubility of CO_2 in chloride solutions at elevated temperatures and CO_2 pressures. *Geochem. Int.* **1975**, *12*, 199−201.
(15) Prutton, C. F.; Savage, R. L. The solubility of carbon dioxide in calcium chloride—water solutions at 75, 100, 120 °C and high pressures. *J. Am. Chem. Soc.* **1945**, *67*, 1550−1554.
(16) Liu, Y.; Hou, M.; Yang, G.; Han, B. Solubility of CO_2 in aqueous solutions of NaCl, KCl, $CaCl_2$ and their mixed salts at different temperatures and pressures. *J. Supercrit. Fluids.* **2011**, *56*, 125−129.
(17) Rumpf, B.; Maurer, G. An experimental and theoretical investigation on the solubility of carbon dioxide in aqueous-solutions of strong electrolytes. *Ber. Bunsen. Phys. Chem.* **1993**, *97*, 85−97.
(18) Bermejo, M. D.; Martin, A.; Florusse, L. J.; Peters, C. J.; Cocero, M. J. The influence of Na_2SO_4 on the CO_2 solubility in water at high pressure. *Fluid Phase Equilib.* **2005**, *238*, 220−228.
(19) Brunner, G.; Peter, S.; Wenzel, H. Phase equilibrium in the systems *n*-heptane-nitrogen, methylcyclohexane-nitrogen and n-heptane-methylcyclohexane-nitrogen at high pressures. *Chem. Eng. J.* **1974**, *7*, 99−104.
(20) Pawlikowskl, E. M.; Newman, J.; Prausnltz, J. M. Phase equilibriums for aqueous solutions of ammonia and carbon dioxide. *Ind. Eng. Chem. Proc. Des. Dev.* **1982**, *21*, 764−770.
(21) Marteau, Ph.; Tobaly, P.; Ruffier-Meray, V.; Barreau, A. In situ determination of high pressure phase diagrams of methane-heavy hydrocarbon mixtures using an infrared absorption method. *Fluid Phase Equilib.* **1996**, *119*, 213−230.
(22) Tan, J.; Xu, J.; Wang, K.; Luo, G. Rapid measurement of gas solubility in liquids using a membrane dispersion microcontactor. *Ind. Eng. Chem. Res.* **2010**, *49*, 10040−10045.
(23) Maurer, G.; Pérez-Salado Kamps. Á. *Developments and Applications in Solubility*; Letcher, T. M., Ed.; RSC Publishing: Cambridge, 2007.
(24) Ruffine, L.; Trusler, J. P. M. Phase behaviour of mixed-gas hydrate systems containing carbon dioxide. *J. Chem. Thermodyn.* **2010**, *42*, 605−611.
(25) Wagner, W.; Pruß, A. The IAPWS formulation 1995 for the thermodynamic properties of ordinary water substance for general and scientific use. *J. Phys. Chem. Ref. Data* **2002**, *31*, 387−535.
(26) Hoyt, S. L. Ed. *ASME Handbook on Metal Properties*; McGraw-Hill: New York, 1956.
(27) Li, X.; Boek, E.; Maitland, G. C.; Trusler, J. P. M. Interfacial tension of (brines + CO_2): (0.864 NaCl + 0.136 KCl) at temperatures between (298 and 448) K, pressures between (2 and 50) MPa, and total molalities of (1 to 5) mol·kg^{-1}. *J. Chem. Eng. Data* **2012**, *57*, 1078−1088.
(28) Li, X.; Boek, E.; Maitland, G. C.; Trusler, J. P. M. Interfacial tension of (brines + CO_2): $CaCl_2$(aq), $MgCl_2$(aq), and Na_2SO_4(aq) at temperatures between (343 and 423) K, pressures between (2 and 50) MPa, and molalities of (0.5 to 5) mol·kg^{-1}. *J. Chem. Eng. Data* **2012**, *57*, 1369−1375.
(29) Lubetkin, S. D.; Akhtar, M. The variation of surface tension and contact angle under applied pressure of dissolved gases, and the effects of these changes on the rate of bubble nucleation. *J. Colloid Interface Sci.* **1996**, *180*, 43−60.
(30) Span, R.; Wagner, W. A new equation of state for carbon dioxide covering the fluid region from the triple-point temperature to 1100 K at pressures up to 800 MPa. *J. Phys. Chem. Ref. Data* **1996**, *25*, 1509−1596.
(31) *EA4−02, Expression of the Uncertainty of Measurement in Calibration*; European Co-operation for Accreditation: Utrecht, 1999.
(32) Wiebe, R.; Gaddy, V. L. The solubility in water of carbon dioxide at 50, 75 and 100°, at pressures to 700 atm. *J. Am. Chem. Soc.* **1939**, *61*, 315−318.
(33) Hou, S.-X.; Maitland, G. C.; Trusler, J. P. M. Measurement and modeling of the phase behavior of the (carbon dioxide + water) mixture at temperatures from 298.15 to 448.15 K. *J. Supercrit. Fluids* **2013**, *73*, 87−96.
(34) Duan, Z. H.; Sun, R.; Zhu, C.; Chou, I. An improved model for the calculation of CO_2 solubility in aqueous solutions containing Na^+, K^+, Ca^{2+}, Mg^{2+}, Cl^-, and SO_4^{2-}. *Mar. Chem.* **2006**, *98*, 131−139.
(35) Duan, Z. H.; Sun, R. An improved model calculating CO_2 solubility in pure water and aqueous NaCl solutions from 273 to 533 K and from 0 to 2000 bar. *Chem. Geol.* **2003**, *193*, 257−271.
(36) Pentland, C. H.; El-Maghraby, R.; Georgiadis, A.; Iglauer, S.; Blunt, M. J. Immiscible displacements and capillary trapping in CO_2 Storage. *Energy Procedia* **2011**, *4*, 4969−4976.
(37) Al Ghafri, S.; Maitland, G. C.; Trusler, J. P. M. Densities of aqueous $MgCl_2$(aq), $CaCl_2$(aq), KI(aq), NaCl(aq), KCl(aq), $AlCl_3$(aq), and (0.964 NaCl + 0.136 KCl)(aq) at temperatures between (283 and 472) K, pressures up to 68.5 MPa, and molalities up to 6 mol·kg^{-1}. *J. Chem. Eng. Data* **2012**, *57*, 1288−1304.
(38) Sako, T.; Hakuta, T.; Yoshltome, H. Vapor pressures of binary (water-hydrogen chloride, -magnesium chloride, and -calcium chloride) and ternary (water-magnesium chloride-calcium chloride) aqueous solutions. *J. Chem. Eng. Data* **1985**, *30*, 224−228.
(39) Patel, B. H.; Paricaud, P.; Galindo, A.; Maitland, G. C. Prediction of the salting-out effect of strong electrolytes on water + alkane solutions. *Ind. Eng. Chem. Res.* **2003**, *42*, 3809−3823.
(40) Harvey, A. H. Semiempirical correlation for Henry's constant over large temperature ranges. *AIChE J.* **1996**, *42*, 1491−1494.
(41) Carroll, J. J.; Mather, A. E. The system carbon dioxide−water and the Krichevsky−Kasarnovsky equation. *J. Sol. Chem.* **1992**, *21*, 607−621.
(42) O'Connell, J. P.; Sharygin, A. V.; Wood, R. H. Infinite dilution partial molar volumes of aqueous solutes over wide ranges of conditions. *Ind. Eng. Chem. Res.* **1996**, *35*, 2808−2812.